

## 3D-Simulations of Transverse Optical Modes of the Free Electron Laser Resonator with Hole Output Coupling

Yu-Huan Dou\*, Xiao-Jian Shu and Yuan-Zhang Wang

*Institute of Applied Physics and Computational Mathematics, P.O. Box 8009, Beijing 100088, P.R. China.*

Received 29 September 2005; Accepted (in revised version) 26 April 2006

---

**Abstract.** The transverse construction of optical modes in the wiggler is calculated and the numerical simulations of the free-electron laser hole-coupled resonator are carried out. These 3D-simulations include optical amplitude distributions, modes evolution of optical field and the influence of hole-radius on the distributing of modes. The numerical simulations confirm that the fraction of the even-order modes increase in the start-up stage and then decreases in the exponential gain stage. Moreover, it is found that the fundamental mode is dominant in the saturate stage. Based on this observation, we estimate the optical output coupling by using the the fundamental mode. It is found that the numerical results and the first-order estimate are in good agreement for a range of the hole size.

**Key words:** Free-electron laser; optical resonator; mode analysis; numerical simulation.

---

### 1 Introduction

Output hole has important impact on the structure of transverse optical modes. It also introduces many difficulties in calculating the optical loss and output coupling. The earlier theory [1, 2] studied the characters of transverse optical modes to the cold-cavity case using the Fox-Li procedure [3]. In general, the results are in good agreement with the experimental ones for gas laser and chemistry laser due to the fact that the corresponding medium is uniform in the intercavity. However, for free electron laser (FEL) system, the radius of the electron beam is very slim, and the gain and the optical guiding from electron beam make the loaded and unloaded cavity cases very different. For example, Pantell et

---

\*Correspondence to: Yu-huan Dou, Institute of Applied Physics and Computational Mathematics, P.O. Box 8009, Beijing 100088, P.R. China. Email: yuhuan\_dou@yahoo.com.cn

al. [4] and Xie and Kim [5] observed that many modes can coexist in the cold-cavity of FEL, but this is not true in the loaded FEL cavity case. Krishnagopal et al. [6] and Faatz et al. [7] carried out 2D-simulations to the FEL hole-coupled resonator considering the influence of the electron beam. The profiles of the optical modes were simulated in [8]. The three-dimensional (3D) simulations of a waveguide FEL oscillator was done by Shu et al. [9]. Recently, some new optical resonators of FEL have been developed, see, e.g., [10,11]. For short Rayleigh length FEL resonator, Blau et al. [12] investigated the problem of the optical mode distortion. From the point of view of modes, the research of the interaction of optical and electron beam is useful in understanding the rule of FEL hole-coupled resonator and for adjusting the hole-size in the experiments.

In this work, we will study the transverse optical modes of the FEL hole-coupled resonator by using our FEL oscillator codes (3-DOSIFEL) [13,14]. To our knowledge, there have been very few detailed 3D simulations in this direction. The paper is organized as follows. Firstly the optical modes are estimated by some series expansion methods. Then the transverse construction of optical modes in the wiggler is calculated for the FEL hole-coupled resonator with the consideration of the gain and optical guiding effects. These 3D-simulations include amplitude distributions and modes evolvment of optical fields, and the distributing of modes in the entrance and on the mirrors as a function of the hole-radius. The transverse construction of the optical field will be determined by the gain and optical guide of the electron beam, and the diffraction and the hole coupling output. The numerical simulations confirm that the proportion of the high-order modes will increase in the start-up stage then decrease in the exponential gain stage. Moreover, the fundamental mode is dominant in the saturate stage. Based on these facts, the estimate for the optical output coupling is obtained by using approximations for the fundamental modes.

## 2 The estimate of the optical modes

The transverse spread of optical modes can be expressed as

$$E_s(x, y, z) = \sum_{m,n=0}^{\infty} A_{mn}(z)g_{mn}(x, y, z). \quad (2.1)$$

For ordinary FEL system, the stable cavity consists of two concave mirrors. The transverse modes  $g_{mn}$  are composed of the products of Hermite-Gaussian modes in the  $x$ -direction and  $y$ -direction [15].

Consider the interaction between electron beam and optical beam. It can be obtained from the resonant condition that

$$\frac{d}{dt} [(k_w + k_z)z - \omega t - (m + n + 1) \tan^{-1}(z/z_r)] = 0, \quad (2.2)$$

where  $dz/dt = \beta_z c$  and  $\omega = 2\pi\nu_{mn}$ . It can be deduced that at  $z = 0$

$$v_{mn} = \frac{\varepsilon_{mn}\beta_z c}{\lambda_w(1 - \beta_z)} = \frac{2\varepsilon_{mn}\beta_z c \gamma_z^2}{\lambda_w}, \quad \varepsilon_{mn} = (m + n + 1) \frac{1}{k_w z_r}. \quad (2.3)$$

The electron-beam and wiggler parameters used are listed in Table 1. The frequency of mode can be calculated from the formula (2.3):

$$\begin{aligned} v_{0,0} &= 124.41c, & v_{0,1} &= 123.66c, & v_{0,2} &= 122.91c, \\ v_{1,2} &= 122.16c, & v_{2,2} &= 121.41c, & v_{2,3} &= 120.66c. \end{aligned} \quad (2.4)$$

The corresponding comparative ratios of the high order mode and the fundamental mode calculated from the formula  $(v_{m,n} - v_{0,0})/v_{0,0}$  are 0, -0.6%, -1.2%, -1.8%, -2.41% and -3.02%, respectively. Here the gain breadth of the FEL is  $1/2N_u$  which is about 1%. Therefore only very few modes can be excited. If the electron beam is injected without misalignment, then the overlapping factor between the odd-order modes and the electron beams will be zero due to the asymmetry of the Hermite polynomials. Consequently, the odd-order modes cannot be simulated. The primary modes can be simulated are the fundamental modes and the even-order modes.

### 3 The numerical simulations

The simulations are based on the 3-D FEL oscillator code (3-DOSIFEL) [13, 14] which is developed in our institute in 1995. The function of the code is similar to that of the 3-DFELEX code in LANL. The dependability of the code has been done in [14]. In this work, the code is modified to simulate the construction of the optical modes.

#### 3.1 Basic equations and initial conditions

The 3-D FEL equations are composed of the electronic motion equations and the optical field equations. The electron and optical coupling equations can be obtained following the single-particle theory of FEL, see, e.g., [16–21]. We assume that the  $x$ -direction is perpendicular to the magnetic field, and the  $y$ -direction is parallel to the magnetic field.

The electronic energy and phase equations. The electronic energy and phase equations are given by

$$\frac{d\gamma}{dz} = - \sum_n \frac{\omega F_u a_w |a|}{2c\gamma\beta_z} \sin(\theta + \phi), \quad (3.1)$$

$$\frac{d\theta}{dz} = k_w + k - \frac{\omega}{c} - \frac{\omega}{c\beta_z(1 + \beta_z)\gamma^2} \left\{ 1 + \frac{1}{2}a_w^2 + \frac{1}{2}|a|^2 - F_u a_w |a| \times \cos(\theta + \phi) + \gamma^2 \beta_{\perp\beta}^2 \right\}, \quad (3.2)$$

where  $a_w = eA_w/(mc^2)$ ,  $a = |a|e^{i\phi}$ ,  $u = \omega a_w^2/(8c\gamma^2 k_w)$ ,  $F_u = J_0(u) - J_1(u)$ ,  $k_w = 2\pi/\lambda_w$ ,  $\omega = 2\pi c/\lambda_s$ ,  $\lambda_w$  is the period of wiggler,  $\lambda_s$  the optical wavelength,  $c$  the velocity of light

Table 1: The parameters of CAEP FIR FEL.

<b>Electron beam</b>		<b>Wiggler</b>	
Energy (MeV)	6.5	Period (cm)	3.0
Peak current (A)	5	Peak field strength (kG)	3.0
Micro bunch (ps)	20	Number of periods	50
Emittance ( $\pi$ mm mrad)	1.5	<b>Optical</b>	
Energy spread (%)	0.5	Wavelength ( $\mu$ m)	110
<b>Beam duct</b>		Cavity length (m)	2.536
Length (m)	1.5m	Mirror curvature (m)	1.768

in vacuum,  $\theta$  and  $\phi$  are the phase of electron and optical field, respectively,  $e$  and  $m$  the electron charge and mass, respectively, and  $\gamma$  and  $\beta_{\perp\beta}$  the energy and betatron velocity of the electron, respectively.

The equations for the betatron motion. The equations for the betatron motion of an electron are

$$\frac{d^2x}{dz^2} = -k_{\beta x}^2 x, \quad \frac{d^2y}{dz^2} = -k_{\beta y}^2 y, \quad (3.3)$$

where  $k_{\beta x}^2 = (a_w k_x / \gamma)^2$  and  $k_{\beta y}^2 = (a_w k_y / \gamma)^2$ .

The optical field equations. The optical field equation with the source is:

$$\left( \frac{\partial^2}{\partial x^2} + \frac{\partial^2}{\partial y^2} + 2ik \frac{\partial}{\partial z} \right) a_s = -\frac{4\pi e}{mc^3} \frac{I}{\Delta S} \left\langle F_u a_{wx} \frac{e^{-i\theta}}{\gamma \beta_z} \right\rangle, \quad (3.4)$$

where  $\langle \rangle$  represents the average over electrons, and  $I$  is the current of electron beam. The optical field equation without the sources describes the optical beam transmits without the interaction with the electron beam. In fact, we can solve the problem by setting the right of equation (3.4) to be zero. But the radius of the optical beam on the mirror is larger than that in the middle of the wiggler. It is necessary to add more griddings and take longer simulation time to ensure the correctness of the simulation results. Therefore, for simplicity and efficiency we use the variation radius of the optical beam to make unitary coordinate. In other words, the breadths of the gridding in the middle and the end of the resonator are the same in the new coordinate system. The optical field equation without the sources can be expressed as [14, 19]

$$\frac{\partial^2 E_c}{\partial \bar{x}^2} + \frac{\partial^2 E_c}{\partial \bar{y}^2} \pm 2i \frac{\partial^2 E_c}{\partial \bar{z}^2} + [2 - (\bar{x}^2 + \bar{y}^2)] E_c = 0, \quad (3.5)$$

where  $\bar{x} = \sqrt{2}x/w_z$ ,  $\bar{y} = \sqrt{2}y/w_z$  and  $\bar{z} = z$ . The '+' and '-' signs denote the transmission direction of the optical beam. Then the optical field  $E$  is given by  $E = E_0 E_c \exp [(\bar{x}^2 + \bar{y}^2)/2]$ , where  $E_0$  is the solution of the Gaussian fundamental mode. Thus, the 3-DOSIFEL code is compiled using above equations. In the end of wiggler, the value of the optical field is transformed from the  $(x, y, z)$  coordinate system to the  $(\bar{x}, \bar{y}, \bar{z})$

coordinate system. Then in the entrance of wiggler of the next pass, the contradictory transform is set to be the  $(x, y, z)$  coordinate system. On the mirror, the initial value is decided by the condition of reflection. After many optical passes, the optical power will saturate and the simulation is ended.

**The initial conditions.** In simulations, the distribution functions of the transverse position, velocity, and the energy of the electron are assumed to be Gaussian. The corresponding initial values of the sample electrons are given by Monte Carlo method and the initial phases are loaded according to the 'quiet start' scheme to eliminate the numerical noise. The energy spread means FWHM and the emittance means RMS. The emittance in the  $y$ -direction is the same as that in the  $x$ -direction, and the initial size of the electron beam is chosen to obtain a circular cross-section at the center of the wiggler [19]. The initial distribution of the optical field is given by the fundamental mode.

### 3.2 Optical mode analysis

In the FEL gain course, the mode proportion in the intercavity optical power is different. Here, we will extract the optical power in the course of simulation and calculate the proportion of each mode. It follows from (2.1) that

$$\int_{\bar{y}} \int_{\bar{x}} E_s(\bar{x}, \bar{y}, z) g_{lq}^* d\bar{x} d\bar{y} = \int_{\bar{y}} \int_{\bar{x}} \sum_m \sum_n A_{mn} g_{mn} g_{lq}^* d\bar{x} d\bar{y}. \quad (3.6)$$

The coefficients  $A_{mn}$  is obtained by using the orthogonal properties of the Hermite functions,

$$A_{mn} = \frac{w^2}{2^{m+n} \pi m! n!} \int_{\bar{y}} \int_{\bar{x}} E_s(\bar{x}, \bar{y}, z) g_{mn}^*(\bar{x}, \bar{y}, z) d\bar{x} d\bar{y}. \quad (3.7)$$

The optical field of the  $mn$ -order mode  $E_{mn}$  is given by

$$E_{mn}(\bar{x}, \bar{y}, z) = \frac{w^2}{2^{m+n} \pi m! n!} g_{mn} \int_{\bar{y}} \int_{\bar{x}} E_s(\bar{x}, \bar{y}, z) g_{mn}^*(\bar{x}, \bar{y}, z) d\bar{x} d\bar{y}. \quad (3.8)$$

The intercavity optical power  $P_s$  is

$$P_s = C \int_{\bar{x}} \int_{\bar{y}} |E_s(\bar{x}, \bar{y}, z)|^2 d\bar{x} d\bar{y}, \quad (3.9)$$

where  $C$  is constant, and the optical power of the  $mn$ -order mode  $P_{mn}$  is

$$P_{mn} = C \int_{\bar{x}} \int_{\bar{y}} |E_{mn}(\bar{x}, \bar{y}, z)|^2 d\bar{x} d\bar{y}. \quad (3.10)$$

Their ratio  $f_{mn}$  is given by

$$f_{mn} = \frac{P_{mn}}{P_s} = \frac{\int_{\bar{x}} \int_{\bar{y}} |E_{mn}(\bar{x}, \bar{y}, z)|^2 d\bar{x} d\bar{y}}{\int_{\bar{x}} \int_{\bar{y}} |E_s(\bar{x}, \bar{y}, z)|^2 d\bar{x} d\bar{y}}. \quad (3.11)$$

Using (3.11) we can obtain the values of  $f_{mn}$  and then know the mode evolvments.

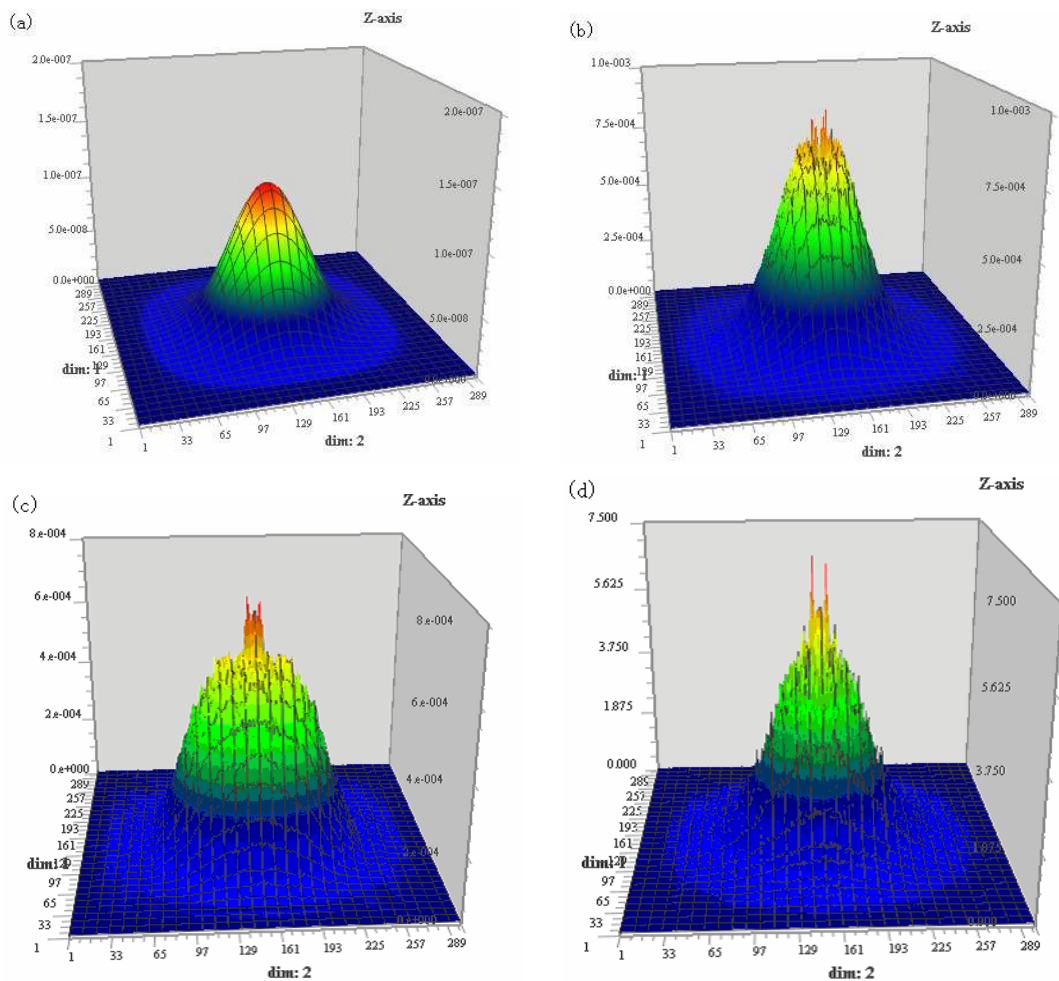


Figure 1: Plots of the amplitude of the optical field in the  $x$  and  $y$  plane. (a) the entrance of the wiggler, pass=1; (b) the exit of wiggler, pass=20; (c) the output mirror, pass=20; and (d) the output mirror after the saturation.

### 3.3 The simulation results

In Fig. 1, the amplitude of the optical field in the  $x$  and  $y$  plane are plotted at different stages and different positions of the optical resonator. Fig. 1(a) shows the distribution of the initial optical field given by the fundamental mode. With the development of the optical field, the distribution becomes spiny as shown in Figs. 1(b) and 1(c). It can be seen from Fig. 1(c) that the peak value is higher in the center of the optical field due to the gain. It is also observed that the radius of the optical field becomes larger in the mirror due to the diffraction and the high-order modes increase. Fig. 1(d) is the plot of the amplitude of the optical field on the output mirror after the saturation. By comparing Figs. 1(c) and 1(d), it is seen clearly that the radius is smaller due to the decreasing of

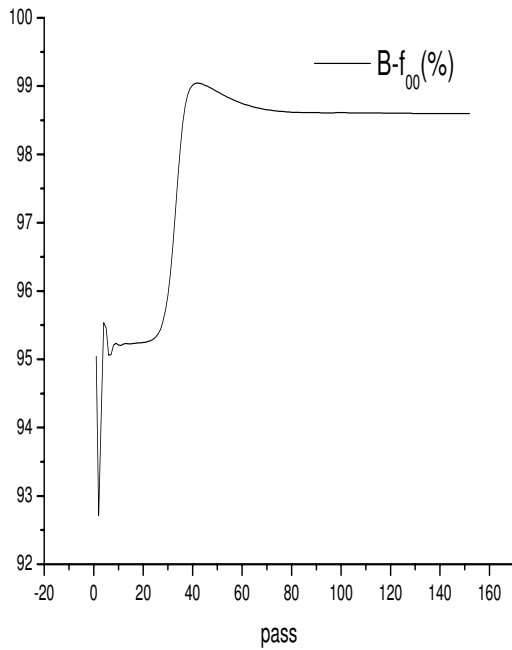


Figure 2: The evolution curves of fundamental mode as a function of optical pass in the exit of wiggler.

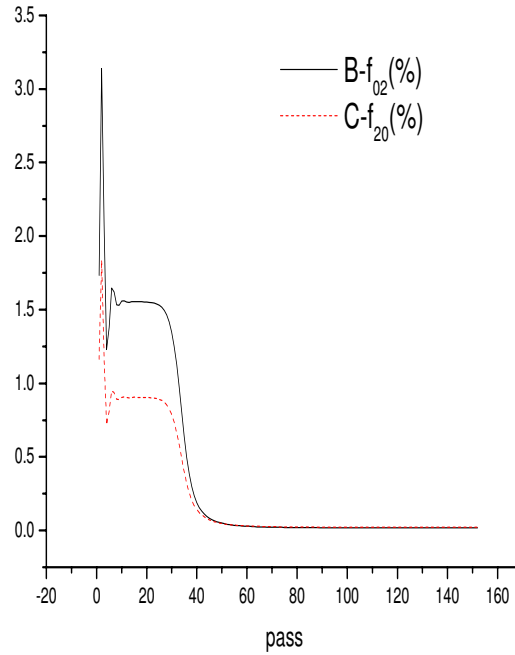


Figure 3: The evolution curves of even-order modes ( $f_{02}$  and  $f_{20}$ ) as a function of optical pass in the exit of wiggler.

the high-order modes.

The mode evolution in optical field is also simulated, and the results are shown in Figs. 2 and 3. It is seen from 2 that the fundamental mode decreases in the start-up stage, increases in the gain stage, and stabilizes (about 98%) in the saturated stage. Fig. 3 presents the evolution curves of two even-order modes,  $f_{02}$  and  $f_{20}$ , as a function of optical pass in the exit of wiggler. For larger pass, the high-order modes will be decreasing due to their smaller gain and larger loss, as shown in Fig. 3. It is concluded that the fundamental mode is dominant in the saturate stage.

The influence of the hole-radius on the distributing of modes is simulated in the entrance and on the mirrors. The results are shown in Tables 2-4. They are the distributing of modes in the entrance and on the mirrors as a function of the hole-radius  $r$ . It can be seen from Tables 2 and 3 that the loss of fundamental mode will increase with respect to the hole-radius. When the hole-radius is 0.3cm, the proportion of the fundamental mode will alter from 96.8% to 81% after the reflection on the output mirror. Because of the asymmetry of the Hermite functions the odd-order modes cannot be stimulated. The proportions of the even-order modes will increase with the increasing hole-radius as shown in Table 2. When the hole-radius is 0.3cm, the proportion of fundamental mode is 81% after being reflected, and becomes 93.6% in the entrance of the wiggler due to the large loss of the high-order modes in the course of transmission, and then becomes 96.8% due to the higher gain as shown in Tables 4 and 2. The transverse construction of the optical field

Table 2: The transverse mode constructions of incident light on the output mirror.

r/cm	$f_{00}$ /%	$f_{01}$ /%	$f_{10}$ /%	$f_{02}$ /%	$f_{20}$ /%	$f_{22}$ /%	$f_{04}$ /%	$f_{40}$ /%
0.06	98.6	1.78E-6	1.81E-5	0.0175	0.0219	3.15E-3	0.080	0.060
0.09	98.7	1.76E-6	2.41E-5	0.0199	0.0227	2.91E-3	0.062	0.048
0.12	98.3	1.78E-6	2.70E-5	0.0221	0.0224	2.29E-3	0.043	0.035
0.18	98.0	2.50E-6	7.33E-5	0.0272	0.0189	8.25E-4	0.011	0.015
0.21	97.7	3.20E-6	8.61E-5	0.0336	0.0169	9.58E-4	0.0018	0.011
0.24	97.5	3.83E-6	1.25E-4	0.0447	0.0161	2.09E-3	0.0012	0.090
0.27	97.0	4.84E-6	1.52E-4	0.0624	0.0176	4.14E-3	0.015	0.013
0.30	96.8	7.14E-6	1.74E-4	0.0987	0.0270	6.31E-3	0.048	0.026

Table 3: The transverse mode construction of reflective light on the output mirror.

r/cm	$f_{00}$ /%	$f_{01}$ /%	$f_{10}$ /%	$f_{02}$ /%	$f_{20}$ /%	$f_{22}$ /%	$f_{04}$ /%	$f_{40}$ /%
0.06	97.9	9.96E-7	1.67E-5	0.010	0.0072	0.0049	0.11	0.13
0.09	97.1	1.31E-6	2.37E-5	0.0048	0.0044	0.015	0.17	0.18
0.12	95.5	1.83E-6	2.84E-5	0.014	0.017	0.034	0.25	0.27
0.18	91.8	2.39E-6	8.09E-5	0.12	0.13	0.12	0.56	0.58
0.21	89.3	3.19E-6	9.44E-5	0.23	0.25	0.19	0.83	0.83
0.24	86.8	4.38E-6	1.46E-4	0.40	0.43	0.28	1.2	1.1
0.27	83.9	6.18E-6	1.86E-4	0.67	0.68	0.40	1.6	1.5
0.30	81.2	7.88E-6	2.26E-4	1.1	1.0	0.55	2.2	1.9

Table 4: The transverse construction of optical modes in the entrance of wiggler.

r/cm	$f_{00}$ /%	$f_{01}$ /%	$f_{10}$ /%	$f_{02}$ /%	$f_{20}$ /%	$f_{22}$ /%	$f_{04}$ /%	$f_{40}$ /%
0.06	98.4	1.86E-6	2.01E-5	0.072	0.079	0.0033	0.102	0.104
0.09	98.4	2.73E-6	2.92E-5	0.10	0.11	0.0067	0.105	0.104
0.12	97.8	4.01E-6	3.81E-5	0.15	0.15	0.013	0.107	0.104
0.18	97.0	5.09E-6	1.01E-4	0.31	0.31	0.046	0.123	0.112
0.21	96.3	6.61E-6	1.16E-4	0.45	0.44	0.078	0.140	0.122
0.24	95.6	8.84E-6	1.82E-4	0.62	0.61	0.12	0.154	0.129
0.27	94.4	1.18E-5	2.32E-4	0.86	0.84	0.18	0.172	0.138
0.30	93.6	1.31E-5	2.89E-4	1.2	1.2	0.26	0.202	0.155

is determined by the gain and optical guide of the electron beam, the diffraction and the hole coupling output. In general, the fundamental mode is dominant in the intracavity. By considering the output coupling and loss, it is suggested that the suitable range of the hole-radius is 0.06-0.1cm. In this range, the proportion of the fundamental mode is above 97% in the whole intracavity.

#### 4 The calculation of the output coupling

It is suggested from the above numerical simulations that the fundamental mode is the main mode after its competition with other modes. Therefore, it is reasonable to use the

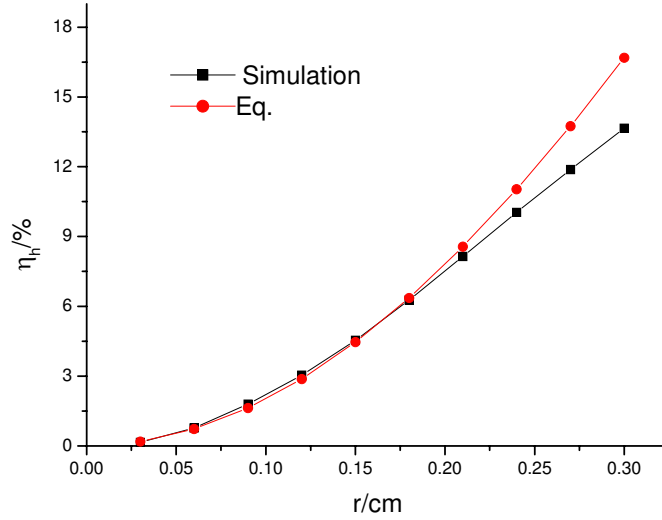


Figure 4: The comparison between simulative and estimative curves of optical output coupling as a function of the hole size.

fundamental mode to estimate the output coupling and other optical cavity characters. Here, the estimate of the optical output coupling is calculated using the approximation for the fundamental mode. The magnitude of unitary optical field can be expressed by

$$\bar{E}_{mn} = \sqrt{\frac{2}{\pi}} \frac{1}{w} \left( \frac{1}{2^{m+n} m! n!} \right)^{\frac{1}{2}} H_m \left( \frac{\sqrt{2}x}{w} \right) H_n \left( \frac{\sqrt{2}y}{w} \right) \exp \left( -\frac{x^2 + y^2}{w^2} + i\theta_{mn} \right). \quad (4.1)$$

The ratio of the output coupling  $\eta_h$  using the fundamental mode is given by

$$\eta_h = \int \int_{\Sigma_h} \bar{E}_{00} \cdot \bar{E}_{00}^* dx dy = 1 - \exp(-2r^2/w^2), \quad (4.2)$$

where  $\Sigma_h$  and  $r$  are the area and the radius of output hole, respectively, and  $w$  is the optical radius in the output mirror.

According to the parameters in Table 1, the size of  $w$  is 0.9929cm. The comparative results between the estimate (4.2) and the simulation are shown in Fig. 4, from which it can be seen that the full numerical and first-order approximation results agree well. When the hole-radius is less than 1.5mm, the numerical result is just slightly larger than the estimative one. When the hole-radius becomes larger, the full numerical result is less than the the result (4.2) due to the involvement of more high-order modes.

## 5 Conclusions

The transverse construction of the optical modes in the wiggler is simulated to the FEL hole-coupled resonator. The results show that the proportion of the even-order modes

increases in the start-up stage and then decreases in the exponential gain stage due to the fact of less gain and more loss. It also demonstrated that the fundamental mode is dominant in the saturate stage. By simulating the influence of the hole-radius on the transverse construction of the optical modes, it is found that the larger the hole-radius is, the higher the proportion of the even-order modes will be. In general, the fundamental mode is dominant in the intracavity. By considering the output coupling and loss, it is suggested that the suitable range of the hole-radius is 0.06-0.1cm to CAEP FIR FEL. Based on these facts, the estimate of the optical output coupling is approximated by using the fundamental mode. The full numerical results and the estimate agree well for small values of the hole-radius.

## References

- [1] G.T. Mcniece, V.E. Derr, IEEE J. Quantum Elect. 5 (1969) 569.
- [2] J.M. Moran, IEEE J. Quantum Elect. 6 (1970) 93.
- [3] A.G. Fox, T. Li, Bell Sys. Tech. J., 40 (1961) 453.
- [4] R.H. Pantell, J. Feinstein, A.H. Ho, Nucl. Instrum. Meth. A296 (1990) 638.
- [5] M. Xie, K.J. Kim, Nucl. Instrum. Meth. A 304 (1991) 792.
- [6] S. Krishnagopal, M. Xie, K.J. Kim, A. Sessler, Nucl. Instrum. Meth. A318 (1992) 661.
- [7] B. Faatz, W.B. Best, P.W. van Amersfoort, D. Oepts, Nucl. Instrum. Meth. A318 (1992) 665.
- [8] R. Prazeres, M. Billardon, Nucl. Instrum. Meth A 318 (1992) 889.
- [9] X.J. Shu, Y.Z. Wang, Y.Q. Jiang, Z.C. Zhang, W. Ding, Nucl. Instrum. Meth. A407 (1998) 76.
- [10] E. Minehara, M. Sawamura, R. Nagai, N. Kikuzawa, M. Sugimoto, R. Hajima, T. Shizuma, T. Yamauchi, N. Nishimori, Nucl. Instrum. Meth. A445 (2000) 183.
- [11] E.A. Antokin, R.R. Akberdin, V.S. Arbutov, M.A. Bokov, V.P. Bolotin, D.B. Burenkov, et al., Nucl. Instrum. Meth. A528 (2004) 15.
- [12] J. Blau, B.W. Williams, S.P. Niles, R.P. Mansfield, FEL2004, Proceedings of the 26th International FEL Conference, Trieste, Italy, 2004, p. 78.
- [13] Z. Wong, Y. Shi, High Power Laser Particle Beams 6(1) (1994) 65, in Chinese.
- [14] T. Wang, Y. Wang, Z. Zhang, J. Yao, High Power Laser Particle Beams 7(1) (1995) 25, in Chinese.
- [15] D. Marcuse, Light Transmission Optics, Van Nostrand, Princeton N. J., 1973.
- [16] B.D. Mcvey, Nucl. Instrum. Meth. A 250 (1986) 449.
- [17] N.M. Kroll, P.L. Morton, M. N. Rosenbluth, IEEE J. Quantum Elect. 17 (1981) 1436.
- [18] E.T. Scharieman J. Appl. Phys. 56(6) (1985) 2154.
- [19] J.W. Strohbehn, Top. Appl. Phys. 25 (1978) 295.
- [20] Z. Zhang, T. Wang, Y. Wang, J. Yao, Z. Yang, High Power Laser Particle Beams 3(2) (1991) 217, in Chinese.
- [21] X. Shu, Y. Wang, Nucl. Instrum. Meth. A 483 (2002) 205.